Desalination and Water Treatment
www.deswater.com
doi: 10.5004/dwt.2020.25807

193 (2020) 381–391
July

Development of a novel method for sodium azide removal from aqueous solution using amberlite IRA-900: batch and column adsorption studies

H. Esfandian[a,*], S. Ghanbari Pakdehi[b,*], M. Cattallany[b]

[a]*Faculty of Engineering Technologies, Amol University of Special Modern Technologies, Amol, Iran, Tel./Fax: (+98) 1144153452; email: hossein.esfandian@gmail.com (H. Esfandian)*
[b]*Faculty of Chemical Engineering, "Malek" University of Technology, Tehran, Iran, emails: sh_ghanbari73@yahoo.com (S. Ghanbari Pakdehi), m.cattallany@gmail.com (M. Cattallany)*

Received 5 September 2019; Accepted 7 March 2020

ABSTRACT

In this work, the adsorption characteristics of amberlite IRA-900 chloride resin (amberlite) for azide ions sorption were investigated. The elimination of azide ions from aqueous solution in the batch and continuous (fixed-bed column) was performed. The optimum conditions in the batch system were found, namely a pH of 6, an amberlite dose of 7 g/L, and a reaction time of 50 min. The kinetics of the process was also investigated with four kinetic models including pseudo-first and second-order, Elovich, and Morris–Weber. The pseudo-second-order model showed better fitting with kinetic data. The Temkin, Dubinin–Radushkevich (D–R), Langmuir, and Freundlich were utilized for isotherm study. The Langmuir equation showed a better fitting of the equilibrium data. amberlite indicated a high capacity for azide elimination from aqueous solutions at different concentrations. High desorption efficiency (for amberlite recovery and recycling) was also obtained using 10% (w/w) NaCl. The recovered amberlite also indicated a high ability to remove the azide ions. In the continuous system (fixed-bed column), the effects of key parameters, namely bed heights and flow rates, were comprehensively studied.

Keywords: Azide; Batch; Fixed bed column; Resin; Regeneration; Sorption

1. Introduction

The removal of hazardous materials (organic pollutants, heavy metals, etc) from water and wastewater is an important issue for various types of industries [1,2]. The sodium azide (NaN_3) production has widely increased during the past decades for application in the automotive industry (such as airbag production). Some studies indicated the toxicity of sodium azide and sodium cyanide during ingestion in the creatures' bodies [3–5]. For the protection of human life, airbag, as a necessary item, is widely utilized in new motor vehicles to provide a safe situation for drivers and passengers in case of an accident. Airbag was first used in the late 1980s. Since then, airbag, as a safety device, has shown considerable popularity in incorporating and is widely used in all types of automobiles. The sodium azide, as the main compound in the airbag system, plays a key role. In recent years, based on motor-vehicle industry demand, the rate of sodium azide production has reached over 5 million kg/y [6–8], and this demand is anticipated to continue for the predictable future. The rapid thermal decomposition of the sodium azide is presented in Eq. (1) [8–10]:

$$NaN_3 \rightarrow Na + \frac{3}{2}N_2 \quad (1)$$

Other applications of sodium azide can be classified in several main fields such as a replacement for methyl bromide

* Corresponding authors.

in pesticides [11], chemical preservative in laboratories, clinics, and hospitals [12,13], and its combination with metals for the production of explosive metal–azide complexes [3]. It was found that in the aqueous phase (pKa = 4.65), the azide ions convert to the hydrazoic acid (HN_3). This volatile acid is classified as a toxic and hazardous material [3,7,14].

Due to the high solubility of sodium azide, this material has a high potential to migrate into streams, sewers, lakes, and groundwater sources [3]. In the literature, it is rare to find studies that present data about the azide components removal from aqueous media. Several common processes are widely applied to remove the azide components from the aqueous phase. One of them is ozonation of hydrazoic acid and the reactions, mechanisms, and kinetics of this process have been widely studied in the literature. It was found that the ozonation has the high potential to convert hydrazoic acid into various nitrogenous compounds such as N_2, NO_2^-, and NO_3^- [15]. The ozonation is also used to remove the alkali metal azides from aqueous media. In this process, alkali metal azides convert to alkali metal nitrate and nitrogen. However, this method (ozonation) did not show high performance for the removal of sodium azide ions from aqueous media in highly alkaline solutions [8]. The mechanism of the hypochlorite/azide reaction in aqueous media was investigated by Betterton et al. [3]. It was found that hypochlorite is not suitable for the azide ions removal from aqueous media due to the toxic chlorine azide intermediate production in the acidic conditions and the low rate under basic conditions [3]. Generally, the application of the sorption process for the removal of azide component from aqueous media can be defined as a suitable and effective technology [2,15].

In the present paper, the elimination of the azide ions by using resin (amberlite IRA-900 chloride), as a promising technology, was investigated. The effects of pH, the dosage of resin, and contact time were evaluated in detail and the isotherm, kinetic, and thermodynamics of this process were also studied. In addition, the effects of different parameters such as bed depth and flow rate in the continuous system (fixed-bed column) were comprehensively studied.

2. Materials and methods

2.1. Materials

The amberlite IRA-900 chloride and NaN_3 applied in this study were purchased from Danesh Shimi Azma Co. (Tehran, Iran). Table 1 presents the structure and properties of this resin [16]. The azide ion concentration was measured by a Dionex 500 Ion Chromatography System. The details of the measurement were presented in the previous work [6].

2.2. Batch adsorption experiments

To obtain the maximum removal efficiency, the effect of the experimental condition (initial concentration, contact time, the dosage of resin, and pH) on the removal of azide ions was evaluated. Isotherm thermodynamic, and kinetics study was performed by the data obtained from batch experiments. The experiments were performed by a flask (the volume of solution was 100 mL) on a magnetic stirrer with a constant rotating speed of 200 rpm. All experiments were done twice and the means of data were reported in this study (the error was <4%). The removal efficiency of azide ions was calculated based on Eq. (2):

Table 1
amberlite IRA-900 chloride

Matrix	Styrene-divinylbenzene (macroreticular) (strongly basic)
Chemical structure	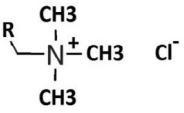
Moisture	55%–65%
Particle size	20–50 mesh (650–820 μm)
Limit temperature	Maximum 65°C
Operating pH	0–14

$$\%\text{Removal} = \frac{C_i - C_f}{C_i} \times 100 \tag{2}$$

where C_i and C_f are the initial and final concentrations (mg/L) of azide ions, respectively.

The sorption capacity at time t, q_t (mg/g), was calculated based on (Eq. 3):

$$q_t = \frac{\left(C_i - C_t\right)V}{m} \tag{3}$$

where C_t (mg/L) is the concentration of azide ions at time t; V and m are the solution volume and the mass of resin (g), respectively.

The q_e (sorption capacity at equilibrium) was obtained by Eq. (4):

$$q_e = \frac{\left(C_i - C_e\right)V}{m} \tag{4}$$

where C_e (mg/L) is the azide ion concentration at equilibrium.

2.3. Column experiments

The removal of azide ions in the continuous system was carried out in a fixed-bed column (Plexiglas) with an i.d. and length of 3 and 35 cm, respectively. The detailed procedure for the column handling is presented elsewhere [17,18]. To achieve the required bed height of the resin, a specified amount of resin was placed in the column. A peristaltic pump (pp40, Miclins) was used to provide the desired flow rate of azide ions solution at the column. Samples collection was done at the exit of the column and then samples were analyzed for azide ions concentration.

The details of the calculations of the M_{ad} (total quantity of azide ions mass sorbed in the column), M_{total} (total amount of azide ions sent to the column), and total azide removal were completely described in our previous study [17–19].

To perform the desorption process and regeneration of resins, 10% (w/w) sodium chloride solution was pumped to the column after being rinsed at the flow rate of 1 mL/min. Other cycles of sorption–desorption and resin regeneration processes were carried out in the same manner as mentioned above.

3. Results and discussion

3.1. Batch adsorption study

3.1.1. Effect of pH

To study the effect of the initial pH on the azide ions concentration, some experiments were carried out with 100 mL of a 1,000 mg/L sodium azide solution containing 0.7 g of the dosage of sorbent (amberlite) (Fig. 1). As can be seen, the azide ions concentration decreased by increasing the pH value. It later reached a minimum value at pH 6 and then increased at higher pH values [20,21].

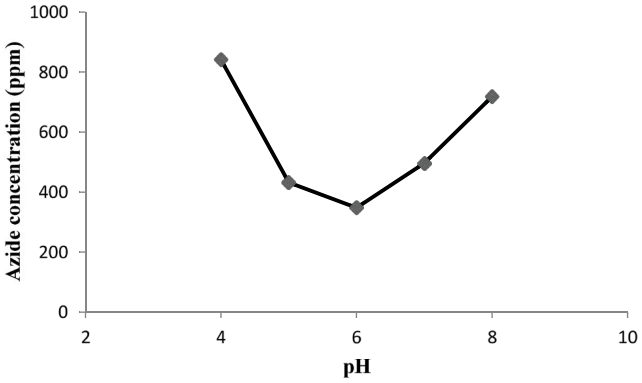

Fig. 1. Effect of the pH on the sorption of azide ions.

3.1.2. Effect of contact time

In batch experiments, optimization of the contact time as one of the important parameters that has a considerable effect on removal efficiency was carried out. The azide ions concentration at various contact times is shown in Fig. 2. During contact-time optimization experiments, initial azide ions concentration, and resin dose were selected to be 1,000 mg/L and 0.7 g in 100 mL, respectively. As can be seen, after 50 min of contact time, azide ions concentration was reduced to 341 ppm. Also, no considerable change in azide ions concentration was observed [22]. Based on the results, a contact time of 50 min was chosen as the optimum contact time and was used for further experiments.

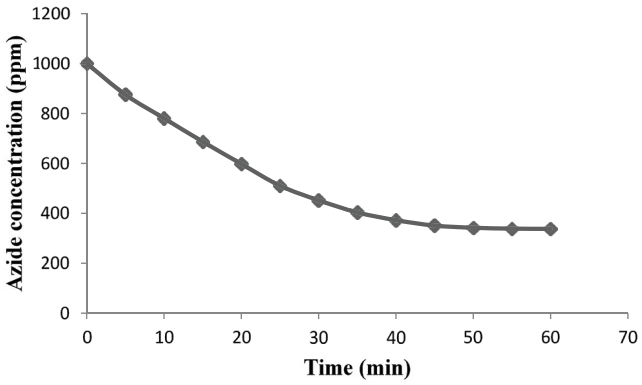

Fig. 2. Effect of the contact time on the sorption of azide ions.

3.1.3. Kinetics of sorption

The physical and chemical characteristics of the sorbent have an important role in the mechanism of sorption. To discuss the main controlling mechanism of azide ions sorption in the case of amberlite, several common sorption kinetic models such as intra-particle diffusion, Elovich, pseudo-first-order, and pseudo-second-order have been applied [21].

3.1.4. Morris–Weber Kinetic model

In batch sorption with stirring, a relationship exists between the diffusive mass transfer and an apparent diffusion coefficient, which will fit the experimental sorption-rate data. The Morris–Weber kinetic model is presented in Eq. (5) [23]:

$$q_t = K_{\mathrm{id}}\left(t\right)^{0.5} + C \tag{5}$$

where C and K_{id} are the intercept and the rate constants (mg/g min$^{1/2}$), respectively. The plot of q_t vs. $t^{0.5}$ is indicated in Fig. 3. As shown in the figure, the plot is linear with a correlation factor of 0.981. The rate constant of the Morris–Weber model, K_{id}, was calculated from the slope of the linear plot (16.99 min^{-1}). Based on this model, the linear

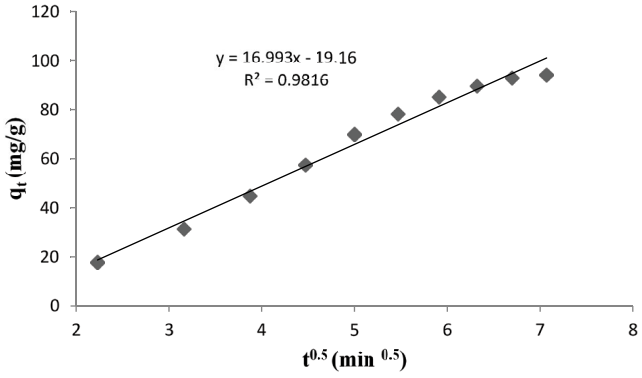

Fig. 3. Morris–Weber plot of azide ions sorption onto amberlite.

plot of q_t vs. $t^{0.5}$ showed that the intraparticle diffusion was one of the mechanisms of adsorption process. It was found that by passing the lines through the origin, the intraparticle diffusion should be considered as a rate-controlling step. When the plots did not pass through the origin, this phenomenon showed that the boundary layer could be an effective parameter in the mechanisms of sorption. It also showed that the intraparticle diffusion parameter is not the only rate-limiting step. Other mechanisms should be considered as an effective parameter for controlling the rate of adsorption [21,23].

The appearance of the linear portion in Fig. 3 clearly indicated the intraparticle diffusion effects [24]. The significant values of the correlation factor (R^2) were calculated using the data from azide ions sorption by resins, demonstrating that the intraparticle diffusion plays a role as a key parameter in the sorption of azide ions by resin. Because of an intercept in the plot (Fig. 3), it was obvious that another mechanism was also involved in the process of sorption of azide ions onto amberlite [25].

3.1.5. Lagergren kinetic model

In 1898, a first-order rate equation was presented by Lagergren for the description of liquid–solid-phase adsorption kinetics (oxalic acid and maleic acid onto charcoal). Based on the adsorption capacity, this model was related to the adsorption rate [26]. This kinetic model can be presented by Eq. (6) [26]:

$$\log\left(q_e - q_t\right) = \log q_e - \left(\frac{K}{2.303}\right)t \tag{6}$$

where K is the Lagergren rate constant for the first-order sorption. The K (rate constant) value was obtained by calculation of the slope of the linear plot of $\log(q_e - q_t)$ vs. time (Fig. 4) [26]. The calculated K value was equal to 0.103 min^{-1} with a correlation factor of 0.921. Based on a low correlation coefficient (R^2 = 0.921), the Lagergren model did not show a well-fitting to experimental data of azide ions sorption onto the resin. The boundary layer or external resistance can be described as the main reason for this poor data fitting [20,21].

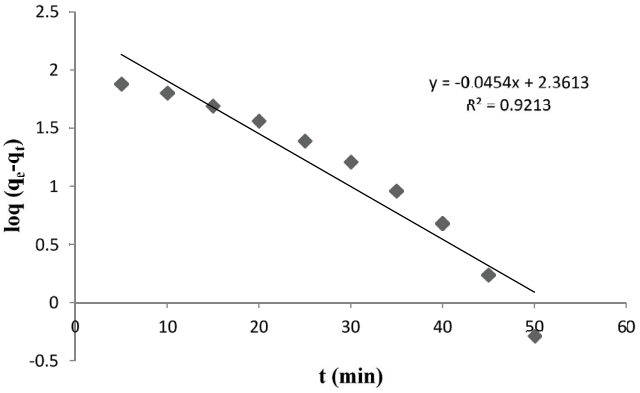

Fig. 4. Validation of Lagergren plot of azide ions sorption onto amberlite.

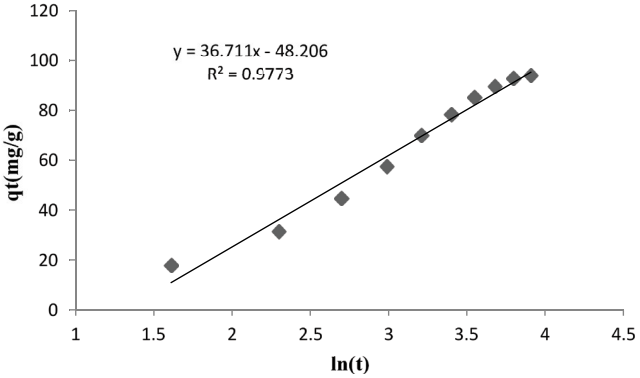

Fig. 5. Elovich plot of azide ions sorption onto amberlite.

3.1.6. Elovich kinetic model

The experimental data were analyzed by the Elovich model [27] which is in linear form as expressed by Eq. (7):

$$q_t = \ln\left(\alpha\beta\right) + \left(\frac{1}{\beta}\right)\ln t \tag{7}$$

where α (mg/g min) and β (g/mg) are defined as the initial rate constant and desorption constant, respectively; β is also related to the chemisorption activation energy. The values of α and β were 6.81 and 0.027, respectively. These values were obtained from the slope and intercept of the plot of q_t vs. ln$t$ (Fig. 5).

The good linearity (R^2 = 0.967) can be discussed to understand the fact that both the initial rate of the process and the nature of sites are key parameters in the sorption process. Two assumptions can be considered: First, the release of energies based on the chemisorptions was related to the extent of coverage. Second, the heterogeneity in the active sites caused the variation in the activation energies during chemisorptions [28].

3.1.7. Pseudo-second order kinetic model

For the first time, Blanchard et al. [29] presented a pseudo-second-order kinetic model in which the sorption capacity of the sorbents was considered as the main parameter. The pseudo-second-order kinetic model is based on the chemisorption and the rate-limiting step in this model should be considered based on the valence forces through sharing or exchanging the electrons between the adsorbent and the adsorbate. The linear form of this model is presented in Eq. (8) [30]:

$$\frac{t}{q_t} = \frac{1}{k_2 q_e^2} + \frac{t}{q_e} \tag{8}$$

In this model, k_2 is the rate constant (g mg^{-1} min^{-1}). The constants can be calculated from the slope of the straight line of plotting (t/q_t) vs. t.

The kinetic study clearly showed a good harmony between the kinetic data and the pseudo-second-order kinetic model (Fig. 6). The assumption behind the pseudo-second-order model suggests that chemisorptions play an important role in the azide ions sorption by resin [31]. Due to the high correlation factor (R^2) of the Morris–Webber, it can also be considered that both the intraparticle diffusion and chemical sorption control the adsorption of azide ions onto amberlite. The lower correlation factor of the intraparticle kinetic model indicated that two important points should be considered: First, the removal of azide ions from aqueous solution is related to the number of azide ions in the solution. Second, there is a relationship between the intraparticle

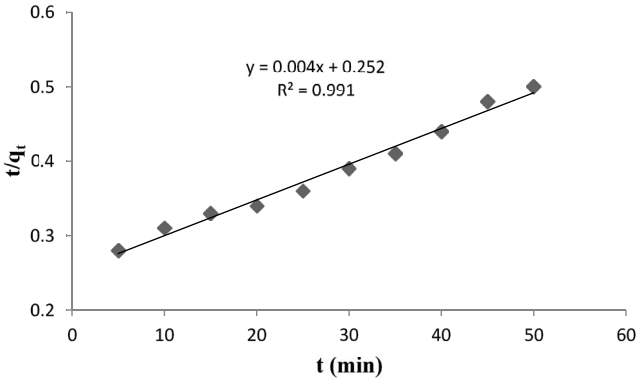

Fig. 6. Pseudo-second-order plot of azide ions sorption onto amberlite.

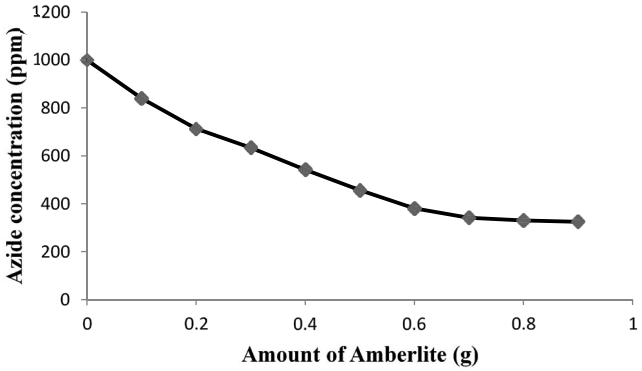

Fig. 7. Effect of the dosage on the azide sorption.

diffusivity and solid-phase concentration [32,33]. It was also reported that the sorption process obeyed first-order and pseudo-second-order kinetics at the high and low initial concentrations of adsorbates, respectively [34].

3.1.8. Effect of dosage of amberlite on azide sorption

The sorption of azide ions as a function of the dosage of sorbent (amberlite) is shown in Fig. 7. The range of the sorbent dosage was selected to be between 0.1 and 0.9 g with an initial azide concentration of 1,000 mg/L at a temperature of 25°C. By increasing the amberlite dose from 0.1 to 0.7 g, the removal of azide ions increased. At a higher dosage of sorbent (greater than 0.7 g), no significant change in the removal of azide ions was observed. It was obvious that a higher dosage of the sorbents provided more available sorption sites. [35].

3.1.9. Effect of the initial concentration of azide on the adsorption

The removal process of the azide ion at a different initial concentration (in the range of 1,000–2,100 mg/L) was investigated at optimum sorbent dosage and contact time (Fig. 8). The sorption capacity of amberlite increased from 94.04 to 150.36 mg/g when the initial azide ions concentration changed in the range of 1,000–1,800 mg/L. For the azide ions concentration greater than 1,800 mg/L, no considerable increase in sorption capacity was observed. The data of different initial concentration (pH, contact time, volume of solution, and amount of adsorbent were 6, 50 min, 100 mL, and 0.7 g, respectively (Fig. 8)) were used to fit different isotherm models, such as Langmuir, Freundlich, Temkin, and Dubinin–Radushkevich (D–R).

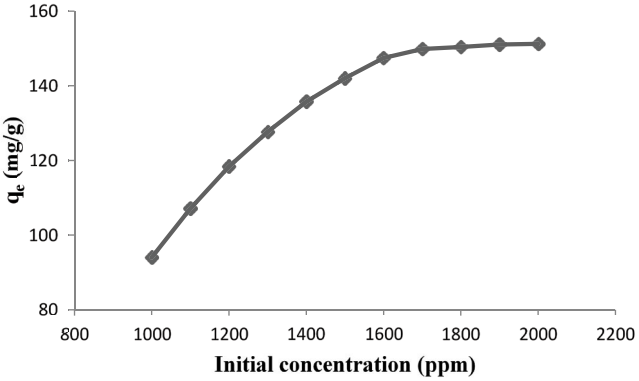

Fig. 8. Effect of the initial concentration on the sorption capacity.

3.1.10. Isotherm model

To demonstrate a successful dynamic adsorptive process for solutes to adsorb onto a sorbent, the equilibrium between the two phases should be comprehensively described. When the amount of solute sorption onto sorbent and solute desorption from sorbent is equal, equilibrium is established [36,37].

3.1.11. Langmuir isotherm model

The Langmuir isotherm model is based on the monolayer adsorption and homogenous surface of the adsorbent [38]. As the main point according to the Langmuir isotherm model, when a site is occupied by a molecule, no further adsorption can occur. It is also assumed that all adsorbents have identical sites and the same energy. This isotherm is presented in Eq. (9):

$$q_e = \frac{q_0 K_L C_e}{1 + K_L C_e} \tag{9}$$

In this equation, q_0 is the theoretical monolayer sorption capacity (mg g^{-1}). The linear form of the Langmuir is presented below (Fig. 9):

$$\frac{C_e}{q_e} = \frac{1}{q_0 K_L} + \frac{1}{q_0} C_e \tag{10}$$

The values q_0 and K_L can be obtained from the slope ($1/q_0$) and intercept (K_L/q_0) of the C_e/q_e vs. C_e plot. The equilibrium parameter R_L (dimensionless constant for the characteristics of the Langmuir) can be defined as Eq. (11):

$$R_L = \frac{1}{1 + K_L C_0} \tag{11}$$

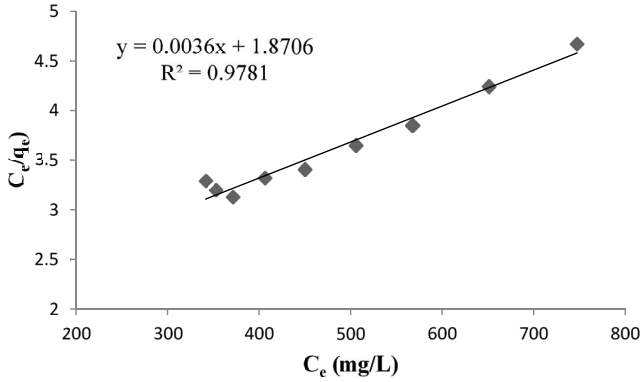

Fig. 9. Langmuir sorption isotherm of azide ions onto amberlite.

where K_L is the Langmuir constant and R_L is shown in Table 2. The R_L value between 0 and 1 shows a favorable sorption process [39]. For concentrations of azide between 1,000 and 1,800 mg/L, the results are presented in Table 3. The Langmuir isotherm showed good fitting with the experimental data which may be due to homogenous distribution of active sites on the amberlite.

3.1.12. Freundlich isotherm model

The Freundlich isotherm model, as an empirical equation, expresses sorption on a heterogeneous surface and assumes a logarithmic decrease in the enthalpy of adsorption with an increase in the fraction of the occupied sites. The equation of the Freundlich isotherm model is presented by Eq. (12) [40]:

$$q_e = K_F C_e^{1/n} \tag{12}$$

In this equation, K_F and $(1/n)$ are the Freundlich constants related to adsorption capacity and the energy or intensity of adsorption, respectively; $(1/n)$ is a heterogeneity factor characterization that makes Freundlich isotherm a suitable model to describe heterogeneous systems [20,41]. To calculate the constants of Freundlich model (K_F and $(1/n)$), the linear form (Eq. (13)) of this equation can be used to plot a graph of $\log(q_e)$ vs. $\log(C_e)$ (Fig. 10):

$$\log q_e = \log K_F + \frac{1}{n}\log C_e \tag{13}$$

The $(1/n)$ and K_F are obtained from the slope and the intercept of the plot, respectively. Also, the data obtained are presented in Table. 3. The n value indicates the favorability of the adsorption process. Generally, $2 < n < 10$ presents good adsorption characteristics whereas $1 < n < 2$ and $n < 1$ express moderately difficult and poor adsorption.

Table 2
Description of type of isotherm by R_L

Type of isotherm	R_L–value
Unfavorable	$R_L > 1$
Linear	$R_L = 1$
Favorable	$0 < R_L < 1$
Irreversible	$R_L = 0$

Table 3
Isotherm constant for azide ions onto amberlite

	Langmuir equation	
K_L	q_0	R^2
328.07	175.43	0.978
	Freundlich parameter	
K_F	n	R^2
5.19	2.37	0.812
	D–R parameter	
q_m	β	R^2
174.16	0.009	0.954
	Temkin parameters	
B	K_T	R^2
64.58	0.01	0.824

3.1.13. Temkin isotherm model

In the Temkin isotherm model, some indirect interactions between adsorbate and adsorbent cause a variation on the isotherm and adsorption process. Due to these interactions, coverage causes a linear decrease in the adsorption heat of all the molecules in the layer [42]. Eq. (14) presents the Temkin model:

$$q_e = B\ln\left(K_T C_e\right) \tag{14}$$

In this model, $B = (RT/A_T)$ and K_T are Temkin constants. A_T (J/mol) is the variation of the adsorption energy between two active sites. T (K) and R (kJ/mol K) are the adsorption temperature and the universal gas constant, respectively. Eq. (14) can be presented in its linear form as Eq. (15):

$$q_e = B\ln K_T + B\ln C_e \tag{15}$$

A plot of q_e vs. $\ln C_e$ is used to calculate the constants A and B (Fig. 11).

The main assumption in the Temkin model is that the adsorption sites in the adsorbent are unequal. This has caused differences in the adsorption energies for each active site [43].

3.1.14. Dubinin–Radushkevich isotherm model

The Dubinin–Radushkevich isotherm model [44], as an empirical isotherm that is initially applied to the subcritical vapors adsorption onto microporous materials, is based on a pore filling strategy. This model is also used to demonstrate the mechanism of adsorption [45] based on a Gaussian energy distribution on heterogeneous surfaces of adsorbents [46].

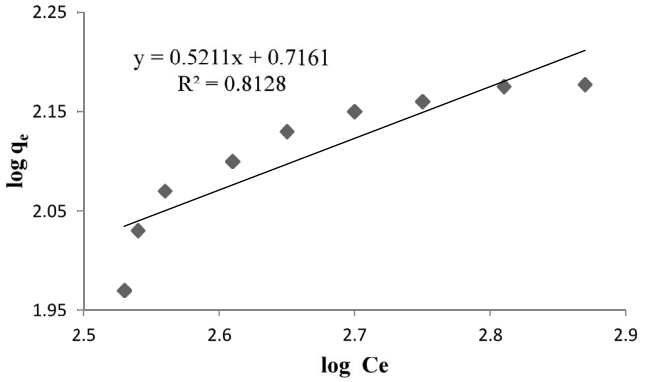

Fig. 10. Freundlich sorption isotherm of azide ions onto amberlite.

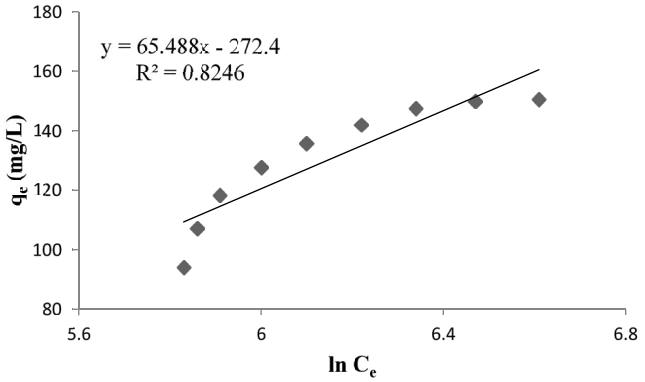

Fig. 11. Temkin sorption isotherm of azide ions onto amberlite.

Eq. (16) expresses the linear form of this model:

$$\ln\left(q_e\right) = \ln\left(q_m\right) - \beta\varepsilon^2 \tag{16}$$

In this equation, q_m and β are the monolayer capacity and the activity coefficient (ascribed to sorption energy of active sites), respectively; ε is the Polanyi potential presented as Eq. (17):

$$\varepsilon = RT\ln\left(1+\frac{1}{C_e}\right) \tag{17}$$

In Eq. (17), R and T are the gas constant (8.314 J/mol K) and absolute temperature (K), respectively. The slope and intercept of the plots of $\ln q_e$ vs. ε^2 (Fig. 12) are used to determine the values β and q_m. The isotherms constants are represented in Table 3. The data of azide sorption onto amberlite show good fitting with Langmuir model (based on the correlation factor), although the D–R equation also shows a considerable correlation factor. The main mechanism for the removal of azide ions from aqueous media by resin is ion exchange, although physical adsorption has also been reported in other literature. Regarding the adsorption part, as the main mechanism for the polyacrylic resins such as amberlite IRA-900, the aromatic rings of the azide ions interacted with a matrix of the anion exchanger. The ion exchange mechanism can be explained

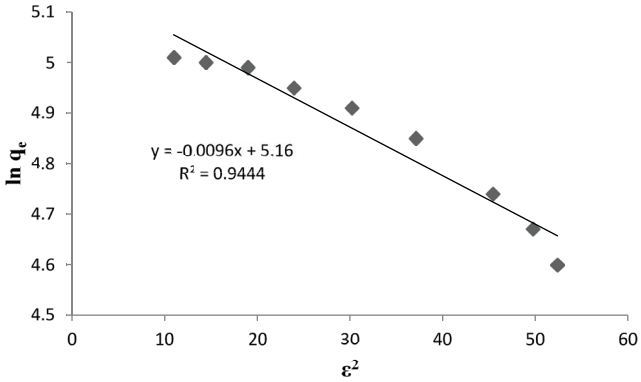

Fig. 12. D–R sorption isotherm of azide ions onto amberlite.

based on the formation of H-bonds between resin and nitrogen of the sodium. The bond formation between the oxygen of the carbonyl group of the resin and the nitrogen of the sodium azide can be introduced as another mechanism [47].

3.1.15. Effect of the other anions

To investigate the effect of the other ions on the azide ions sorption by resin, some anions including NO_3^-, F^-, and A^- (humic acid ions) were selected. Two different concentrations of 50 and 100 ppm were selected for the concentration of these anions in azide ion solution. The results are given in Table 4. The presence of these ions had a negative effect on the sorption of azide by resin. As a result, the amount of azide ions sorbed by resin reduced dramatically. It was also found that by increasing the concentration of NO_3^-, F^-, and A^- in the aqueous phase, more reduction in azide ions sorption by resin was observed. As shown previously, the more negative effect of the A^- in comparison with NO_3^- and F^- on the azide sorption is clear. Maybe due to the larger size of the A^- molecules, more sites on the resin structure will be occupied. Thus, more reduction in azide sorption will take place.

3.1.16. Effect of temperature on the azide ions sorption

The thermodynamics of the adsorption was studied by varying the temperatures in the range of 15°C–35°C (at optimum conditions). The removal efficiency percentage increased with the rise in temperature from 15°C to 35°C. By using the data obtained, the thermodynamic parameters such as Gibbs free entropy change (ΔS°), energy change (ΔG°), and enthalpy change (ΔH°) were calculated based on Eqs. (18)–(20). The parameters are presented in Table 5.

$$K_c = \frac{F_e}{1-F_e} \tag{18}$$

$$\log K_c = \frac{-\Delta H}{2.303RT} + \frac{\Delta S}{2.303R} \tag{19}$$

$$\Delta G = -RT\ln K_c \tag{20}$$

Table 4
Effect of the anions on the azide ions sorption on the resin

Concentration of the anions (ppm)	Final concentration of the azide ion in the presence of the NO_3^-	Final concentration of the azide ion in the presence of the F^-	Final concentration of the azide ion in the presence of the A^-
50	425	473	535
100	512	562	687

Table 5
Thermodynamic parameter for adsorption of sodium azide onto amberlite IRA-900

$\Delta H°$ (kJ/mol)	$\Delta S°$ (kJ/mol k)	T (°C)	$\Delta G°$ (kJ/mol)	R^2
11.98	0.046	15	–1.1049	0.9644
		25	–1.698	
		35	–2.3291	

where F_e is the fraction of azid ions sorbed at equilibrium. The positive value of $\Delta S°$ revealed increased randomness at the solid-solution interface during the adsorption. The positive values of $\Delta H°$ showed the endothermic nature of the adsorption process. In addition, the negative values of $\Delta G°$ indicated the spontaneous nature of the adsorption of azide ions on the amberlite IRA-900.

3.1.17. Comparison of the azide ions adsorption capacities using amberlite IRA-900

Table 6 presents the adsorption capacity of the various adsorbents used for the elimination of azide ions from aqueous media. In this study, the adsorption capacity of amberlite IRA-900 was considerably higher than that of the activated carbon magnetic nanocomposite, Laterite, activated carbon prepared from a walnut shell, NaY zeolite, ZSM-5 zeolite, and activated carbon–commercial grade. This comparison indicates that the amberlite IRA-900 has a high capacity to be considered as a suitable adsorbent for azid ions separation on a large scale.

3.2. Continuous adsorption study

3.2.1. Effect of bed height

Sorption of azide ions onto sorbents in the packed bed column is strictly dependent on the quantity of sorbents within the column. The breakthrough curves of azide ions sorption onto amberlite are presented in Fig. 13. The bed heights varied from 10 to 20 cm at a flow rate of 5 mL/min, and the initial azide ions concentration was 1,000 mg/L. As can be seen, by increasing the bed height, an increase in the sorption capacity values and percentage removal efficiencies are observed (Table 7). The same results were observed in other studies [48]. The maximum sorption capacity (117.78 mg/g) for azide ions sorption onto amberlite was observed at a bed height of 20 cm. The improvement of the removal efficiency and sorption capacity with an increase in the bed height can be explained in this way that a longer bed height provided more adorbents (active sites) for the sorption process. Meanwhile, a longer bed height also provided more residence time into the column for azide ions [49,50].

3.2.2. Effect of flow rate

On an industrial scale, the flow rate can be introduced as one of the important parameters for the treatment of water and wastewater in a continuous system [51]. The flow rate in the range of 5–15 mL/min was chosen. In addition, the bed height in the column and the initial azide ions concentration were 20 cm and 1,000 mg/L, respectively. Fig. 14 indicates the effluent azide ions concentration versus reaction time at different flow rates.

As can be seen, the column shows better performance at a lower flow rate. In the first stage, because of the availability and ability of the reaction sites to capture azide ions inside the sites, the removal process was very fast at a lower flow rate. In the next stage, based on the gradual occupancy of these sites, the removal process became less effective. By increasing the flow rate, the breakthrough curve became steeper and breakpoint time and sorbed ions concentration also decreased. The flow rate at a higher value reduced the residence time such that the azide

Table 6
Comparison of the azide ions adsorption capacities using amberlite IRA-900

Adsorbent	Type of azide ions	q_m (mg/g)	Reference
amberlite IRA-900	Sodium azide	175.43	This work
Activated carbon magnetic nanocomposite	Sodium azide	22.22	[55]
Laterite	Sodium azide	70	[56]
Activated carbon prepared from walnut shell	Dimethyl aminoethyl azide	166.67	[52]
NaY zeolite	Dimethyl aminoethyl azide	21.155	[57]
ZSM-5 zeolite	Dimethyl aminoethyl azide	128.568	[57]
Activated carbon–commercial grade	Dimethyl aminoethyl azide	88.028-	[57]

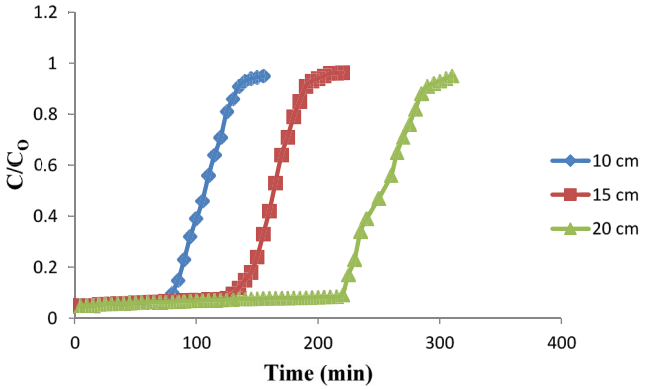

Fig. 13. Breakthrough curves for azide removal from amberlite at different bed heights.

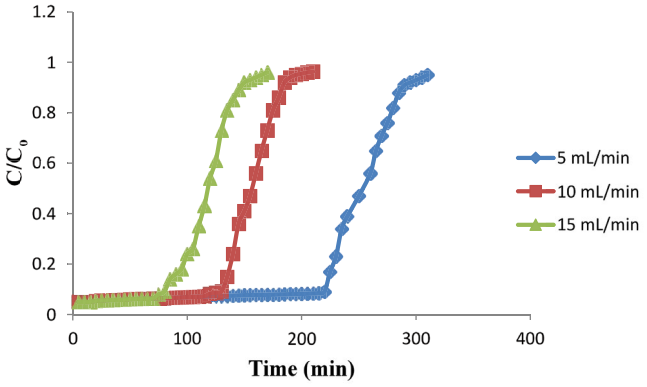

Fig. 14. Breakthrough curves for azide ions removal from amberlite at different flow rates.

Table 7
Data obtained from continuous mode (fixed-bed column) at different bed heights

Bed height	t_b (min)	t_e (min)	M_{total} (mg)	M_{ad} (mg)	q (mg/g)	Removal efficiency (%)
10 cm	80	145	725	541	108.2	74.62
15 cm	125	195	975	774	96.75	79.38
20 cm	220	305	1,525	1,265	117.78	82.95

ions did not have enough time to reach equilibrium [49]. The breakthrough and exhaustion time were dramatically reduced by an increment in the flow rate (Table 8).

3.2.3. Regeneration

The regeneration and reusability of the sorbents are considered as two important parameters for application on an industrial scale. To regenerate the amberlite after its application in azide ions removal, desorption of sorbed azide ions from the amberlite is the main process. It should be noted that any damage or considerable effect on the uptake capacity is not caused by the desorption process [52–54]. In this study, the regeneration process was performed and the sorption–desorption cycle was carried out six times. For this purpose, the column was packed with amberlite with a bed height of 20 cm. A flow rate of 5 mL/min and an azide concentration of 1,000 mg/L were used for the adsorption process. After saturating the amberlite, the regeneration process was performed by the strategy mentioned in the Materials and Methods section.

The column data for all six cycles are presented in Table 9. After the sixth cycle, weight loss of the sorbent was about 5% (a reduction in the bed height was from 20 to 18.35 cm).

Table 8
Data obtained from continuous mode (fixed-bed column) at different flow rates

Flow rate	t_b (min)	t_e (min)
5 mL/min	220	305
10 mL/min	125	195
15 mL/min	75	160

Table 9
Sorption and elution process parameters for six sorption–desorption cycles

Cycle no.	t_b (h)	t_e (h)	q (mg/g)	Removal efficiency (%)
1	220	305	117.78	82.95
2	218	305	115.62	82.16
3	217	303	114.43	81.92
4	214	299	112.72	79.45
5	213	297	111.35	78.47
6	213	296	110.63	78.21

4. Conclusion

This study showed that the amberlite IRA-900 as an anion-exchange resin indicated a considerable potential for the removal of azide ions. The optimum adsorbent dose (g/L), pH, and contact time (min) were 7, 6, and 50, respectively. The equilibrium data were well-fitted by the Langmuir isotherm. By evaluating the kinetic data, controlling the sorption process was carried out by the pseudo-second-order equation. By increasing the initial concentration, a reduction in the removal efficiency was observed. The thermodynamic study showed that the process was endothermic and spontaneous. The results from the column study indicated that an increase in the bed height considerably increased the sorption capacity (mg/g) and removal efficiency, although increasing the flow rates reduced the removal efficiency. Finally, desorption of azide ions from amberlite was studied by using 10% (w/w) NaCl. After the desorption process, the

reduction in the removal efficiency of azide ions by amberlite was negligible (less than 5%).

Acknowledgment

The authors would like to acknowledge Amol University of Special Modern Technologies for all the support.

References

[1] L. Giraldo, A. Erto, J.C. Moreno-Piraján, Magnetite nanoparticles for removal of heavy metals from aqueous solutions: synthesis and characterization, Adsorption, 19 (2013) 465–474.
[2] M.R. Awual, Assessing of lead(III) capturing from contaminated wastewater using ligand doped conjugate adsorbent, Chem. Eng. J., 289 (2016) 65–73.
[3] E.A. Betterton, J. Lowry, R. Ingamells, B. Venner, Kinetics and mechanism of the reaction of sodium azide with hypochlorite in aqueous solution, J. Hazard. Mater., 182 (2010) 716–722.
[4] E.A. Betterton, J.L. Robinson, Henry's law coefficient of hydrazoic acid, J. Air Waste Manage. Assoc., 47 (1997) 1216–1219.
[5] R.P. Smith, D.E. Wilcox, Toxicology of selected nitric oxide-donating xenobiotics, with particular reference to azide, Crit. Rev. Toxicol., 24 (1994) 355–377.
[6] E.A. Betterton, D. Craig, Kinetics and mechanism of the reaction of azide with ozone in aqueous solution, J. Air Waste Manage. Assoc., 49 (1999) 1347–1354.
[7] R. Singh, H.-J. Lee, A.K. Singh, D.-P. Kim, Recent advances for serial processes of hazardous chemicals in fully integrated microfluidic systems, Korean J. Chem. Eng., 33 (2016) 2253–2267.
[8] S.H. Lin, C.P. Huang, Adsorption of hydrazoic acid from aqueous solution by macroreticular resin, J. Hazard. Mater., 84 (2001) 217–228.
[9] E.A. Betterton, technology, Environmental fate of sodium azide derived from automobile airbags, J. Crit. Rev. Environ. Sci., 33 (2003) 423–458.
[10] J.M. Hitt, Automobile Airbag Industry Toxic Exposures, J.B. Sullivan, G.R. Krieger, Eds., Hazardous Materials Toxicology: Clinical Principles of Environmental Health, Williams & Wilkins, Baltimore, MD, 1992, pp. 533–537.
[11] B.M. Santos, J.P. Gilreath, T.N. Motis, J.W. Noling, J.P. Jones, J.A. Norton, Comparing methyl bromide alternatives for soilborne disease, nematode and weed management in fresh market tomato, Crop Prot., 25 (2006) 690–695.
[12] I. Le Blanc-Louvry, P. Laburthe-Tolra, V. Massol, F. Papin, J.P. Goullé, G. Lachatre, J.M. Gaulier, B. Proust, Suicidal sodium azide intoxication: an analytical challenge based on a rare case, Forensic Sci. Int., 221 (2012) e17–e20.
[13] M. Chiba, M. Ohmichi, Y. Inaba, Sodium azide: a review of biological effects and case reports, Nihon Eiseigaku Zasshi, 53 (1999) 572–579.
[14] J.J. Orlando, G.S. Tyndall, E.A. Betterton, J. Lowry, S.T. Stegall, Atmospheric chemistry of hydrazoic acid (HN_3): UV absorption spectrum, $HO^{\bullet}$ reaction rate, and reactions of the $^{\bullet}N_3$ radical, Environ. Sci. Technol., 39 (2005) 1632–1640.
[15] M.R. Awual, New type mesoporous conjugate material for selective optical copper(II) ions monitoring and removal from polluted waters, Chem. Eng. J., 307 (2017) 85–94.
[16] M.R. Awual, A. Jyo, Assessing of phosphorus removal by polymeric anion exchangers, Desalination, 281 (2011) 111–117.
[17] H. Esfandian, A. Samadi-Maybodi, B. Khoshandam, M. Parvini, Experimental and CFD modeling of diazinon pesticide removal using fixed bed column with Cu-modified zeolite nanoparticle, J. Taiwan Inst. Chem. Eng., 75 (2017) 164–173.
[18] H. Esfandiana, B. Khoshandama, M. Parvinia, A. Samadi-Maybodib, An analysis of the sensitivity of fixed bed adsorption for diazinon removal: experimental and modeling studies, Desal. Water Treat., 70 (2017) 330–338.
[19] H. Esfandian, H. Javadian, M. Parvini, B. Khoshandam, R. Katal, Batch and column removal of copper by modified brown algae sargassum bevanom from aqueous solution, Asia-Pac. J. Chem. Eng., 8 (2013) 665–678.
[20] H. Esfandian, M. Parvini, B. Khoshandam, A. Samadi-Maybodi, Artificial neural network (ANN) technique for modeling the mercury adsorption from aqueous solution using *Sargassum bevanom* algae, Desal. Water Treat., 57 (2016) 17206–17219.
[21] H. Esfandian, A. Samadi-Maybodi, M. Parvini, B. Khoshandam, Development of a novel method for the removal of diazinon pesticide from aqueous solution and modeling by artificial neural networks (ANN), J. Ind. Eng. Chem., 35 (2016) 295–308.
[22] S. Senthilkumaar, P. Varadarajan, K. Porkodi, C. Subbhuraam, Adsorption of methylene blue onto jute fiber carbon: kinetics and equilibrium studies, J. Colloid Interface Sci., 284 (2005) 78–82.
[23] W.J. Weber, J.C. Morris, Kinetics of adsorption on carbon from solution, J. Sanitary Eng. Div., 89 (1963) 31–60.
[24] H.L. Ehrlich, C.L. Brierley, Microbial Mineral Recovery, McGraw-Hill, Inc., New York, 1990.
[25] Y.A. Aydın, N.D. Aksoy, Adsorption of chromium on chitosan: optimization, kinetics and thermodynamics, Chem. Eng. J., 151 (2009) 188–194.
[26] Y. Zeroual, B. Kim, C. Kim, M. Blaghen, K. Lee, Biosorption of bromophenol blue from aqueous solutions by Rhizopus stolonifer biomass, Water Air Soil Pollut., 177 (2006) 135–146.
[27] S. Chien, W. Clayton, Application of Elovich equation to the kinetics of phosphate release and sorption in soils†, Soil Sci. Soc. Am. J., 44 (1980) 265–268.
[28] B. Subramanyam, A. Das, Study of the adsorption of phenol by two soils based on kinetic and isotherm modeling analyses, Desalination, 249 (2009) 914–921.
[29] G. Blanchard, M. Maunaye, G. Martin, Removal of heavy metals from waters by means of natural zeolites, Water. Res., 18 (1984) 1501–1507.
[30] H. Ys, G. Mckay, G. Mckay, Pseudo-second order model for sorption processes, Process Biochem., 34 (1999) 451–465.
[31] X. Han, W. Wang, X. Ma, Adsorption characteristics of methylene blue onto low cost biomass material lotus leaf, Chem. Eng. J., 171 (2011) 1–8.
[32] K. Hui, C.Y.H. Chao, S. Kot, Removal of mixed heavy metal ions in wastewater by zeolite 4A and residual products from recycled coal fly ash, J. Hazard. Mater., 127 (2005) 89–101.
[33] X. Yang, S.R. Otto, B. Al-Duri, Concentration-dependent surface diffusivity model (CDSDM): numerical development and application, Chem. Eng. J., 94 (2003) 199–209.
[34] S. Azizian, Kinetic models of sorption: a theoretical analysis, J. Colloid Interface Sci., 276 (2004) 47–52.
[35] D. Kim, Statistical condensation adsorption isotherms of gas molecules adsorbed on porous adsorbents, surface monolayer adsorption isotherms and hysteresis phenomena, Korean J. Chem. Eng., 17 (2000) 600–612.
[36] D.N. Misra, Adsorption on heterogeneous surfaces: a dubinin-radushkevich equation, Surf. Sci., 18 (1969) 367–372.
[37] W. Fritz, E.-U. Schluender, Simultaneous adsorption equilibria of organic solutes in dilute aqueous solutions on activated carbon, Chem. Eng. Sci., 29 (1974) 1279–1282.
[38] I. Langmuir, The adsorption of gases on plane surfaces of glass, mica and platinum, J. Am. Chem. Soc., 40 (1918) 1361–1403.
[39] G. Mckay, H. Blair, J. Gardner, Adsorption of dyes on chitin. I. Equilibrium studies, J. Appl. Polym. Sci., 27 (1982) 3043–3057.
[40] H. Freundlich, Over the adsorption in solution, J. Phys. Chem., 57 (1906) 1100–1107.
[41] H. Moon, W.K. Lee, Intraparticle diffusion in liquid-phase adsorption of phenols with activated carbon in finite batch adsorber, J. Colloid Interface Sci., 96 (1983) 162–171.
[42] M. Temkin, V. Pyzhev, Recent modifications to Langmuir isotherms, Acta Phys. Chim., 12 (1940) 217–225.
[43] S.H. Kim, A. Bidkar, H.H. Ngo, S. Vigneswaran, H. Moon, Adsorption and mass transfer characteristics of metsulfuron-methyl on activated carbon, Korean J. Chem. Eng., 18 (2001) 163–169.
[44] M.M. Dubinin, L.V. Radushkevich, The equation of the characteristic curve of activated charcoal, Dokl. Akad. Nauk., 55 (1947) 327–329.

[45] A. Günay, E. Arslankaya, I. Tosun, Lead removal from aqueous solution by natural and pretreated clinoptilolite: adsorption equilibrium and kinetics, J. Hazard. Mater., 146 (2007) 362–371.
[46] A. Dąbrowski, Adsorption—from theory to practice, Adv. Colloid Interface Sci., 93 (2001) 135–224.
[47] M. Wawrzkiewicz, Anion-exchange resins for CI Direct Blue 71 removal from aqueous solutions and wastewaters: effects of basicity and matrix composition and structure, Ind. Eng. Chem. Res., 53 (2014) 11838–11849.
[48] R. Vimala, D. Charumathi, N. Das, Packed bed column studies on Cd(II) removal from industrial wastewater by macrofungus *Pleurotus platypus*, Desalination, 275 (2011) 291–296.
[49] N. Sylvia, L. Hakim, N. Fardian, Y. Yunardi, Adsorption performance of fixed-bed column for the removal of Fe(II) in groundwater using activated carbon made from palm kernel shells, IOP Conf. Ser.: Mater. Sci. Eng., 334 (2018) 1–9.
[50] S. Srivastava, S. Agrawal, M. Mondal, Fixed bed column adsorption of Cr(VI) from aqueous solution using nanosorbents derived from magnetite impregnated *Phaseolus vulgaris* husk, Environ. Prog. Sustainable Energy, 38 (2019) S68–S76.
[51] D.C. Ko, J.F. Porter, G. McKay, Optimised correlations for the fixed-bed adsorption of metal ions on bone char, Chem.Eng. Sci., 55 (2000) 5819–5829.
[52] S.G. Pakdehi, F. Rezaei, Adsorption of liquid fuel dimethyl amino ethyl azide from dilute aqueous solution on activated carbon prepared from walnut shell, Desal. Water Treat., 57 (2016) 27726–27740.
[53] S. Hasan, D. Ranjan, M. Talat, Agro-industrial waste 'wheat bran'for the biosorptive remediation of selenium through continuous up-flow fixed-bed column, J. Hazard. Mater., 181 (2010) 1134–1142.
[54] B. Volesky, Detoxification of metal-bearing effluents: biosorption for the next century, Hydrometallurgy, 59 (2001) 203–216.
[55] A.R. Zarei, H. Sinapour, Adsorptive removal of azide ion from aqueous solutions using modified activated carbon magnetic nanocomposite, J. Mater. Environ. Sci., 6 (2015) 1297–1303.
[56] A.R. Khataee, S. Ghanbari Pakdehi, Removal of sodium azide from aqueous solution by Fenton-like process using natural laterite as a heterogeneous catalyst: kinetic modeling based on nonlinear regression analysis, J. Taiwan Inst. Chem. Eng., 45 (2014) 2664–2672.
[57] S. Ghanbari Pakdehi, B. Vaferi, A study on adsorptive removal of DMAZ from aqueous solutions by ZSM-5, NaY zeolites, and activated carbon: kinetic and isotherm, Desal. Water Treat., 57 (2016) 18286–18292.